J. Phys. G: Nucl. Part. Phys. **36** (2009) 095001 (15pp) doi:10.1088/0954-3899/36/9/095001

Perspectives of a mid-rapidity dimuon program at the RHIC: a novel and compact muon telescope detector

L Ruan[1], G Lin[2], Z Xu[1], K Asselta[1], H F Chen[3], W Christie[1], H J Crawford[4], J Engelage[4], G Eppley[5], T J Hallman[1], C Li[3], J Liu[5], W J Llope[5], R Majka[2], T Nussbaum[5], J Scheblein[1], M Shao[3], R Soja[1], Y Sun[3], Z Tang[3], X Wang[6] and Y Wang[6]

[1] Brookhaven National Laboratory, Upton, NY 11973, USA
[2] Yale University, New Haven, CT 06520, USA
[3] University of Science & Technology of China, Hefei 230026, People's Republic of China
[4] University of California, Berkeley, CA 94720, USA
[5] Rice University, Houston, TX 77251, USA
[6] Tsinghua University, Beijing 100084, People's Republic of China

E-mail: ruan@bnl.gov

Received 30 April 2009
Published 17 July 2009
Online at stacks.iop.org/JPhysG/36/095001

Abstract

We propose a large-area, cost-effective muon telescope detector (MTD) at mid-rapidity for the solenoidal tracker at the RHIC (STAR) and for the next generation of detectors at a possible electron–ion collider. We utilize large multi-gap resistive plate chambers with long readout strips (long-MRPC) in the detector design. The results from cosmic ray and beam tests show that the intrinsic timing and spatial resolution for a long-MRPC are 60–70 ps and $\sim$1 cm, respectively. The performance of the prototype muon telescope detector at STAR indicates that muon identification at a transverse momentum of a few GeV/c can be achieved by combining information from track matching with the MTD, ionization energy loss in the time projection chamber and time-of-flight measurements. A primary muon over secondary muon ratio of better than 1/3 can be achieved. This provides a promising device for future quarkonium programs and primordial dilepton measurements at the RHIC. Simulations of the muon efficiency, the signal-to-background ratio of J/ψ, the separation of Υ 1S from 2S+3S states and the electron–muon correlation from charm pair production in the RHIC environment are presented.

(Some figures in this article are in colour only in the electronic version)

1. Introduction

Data taken over the last several years have demonstrated that the RHIC has created dense and rapidly thermalizing matter characterized by (1) initial energy densities far above the critical values predicted by lattice QCD for formation of a quark–gluon plasma (QGP); (2) opacity to jets; (3) nearly ideal fluid flow, which is marked by constituent interactions of very short mean free path, established most probably at a stage preceding hadron formation [1]. The next objective at the RHIC is to study properties of this partonic matter in detail in terms of color degrees of freedom and the equation of state. For example, due to color screening, different quarkonium states will dissociate and the dissociation temperatures will be different due to different binding energies. The precise measurement of transverse momentum distributions of quarkonia at different centralities, collision systems and energies will serve as a thermometer of QGP. A large-area muon telescope detector (MTD) at mid-rapidity for RHIC collisions will be crucial for advancing our knowledge of QGP properties. It will directly address many of the open questions and long-term goals proposed in the RHIC white papers [1, 2]. Since muons do not participate in strong interactions, they provide penetrating probes for the strongly interacting QGP. A large area detector identifying muons with momentum of a few GeV/c at mid-rapidity allows for the detection of di-muon pairs from QGP thermal radiation, quarkonia, light vector mesons, possible correlations of quarks and gluons as resonances in QGP and Drell–Yan production, as well as the measurement of heavy flavor hadrons through their semi-leptonic decays into single muons [3]. Some of these topics also can be studied using electrons or photons or a combination of both. However, electrons and photons have large backgrounds from hadron decays, π^0 and η Dalitz decays, and gamma conversions in the detector material. These backgrounds prevent effective triggering in central nucleus–nucleus collisions at mid-rapidity at the solenoidal tracker at the RHIC (STAR). In addition, electron–muon correlation can be used to distinguish between lepton pair production and heavy quark decays ($c+\bar{c} \rightarrow e+\mu(e)$, $B \rightarrow e(\mu)+c \rightarrow e+\mu(e)$). In addition, muons are less affected by bremsstrahlung radiation energy loss in the detector materials than electrons, thus providing excellent mass resolution of vector mesons and quarkonia. This is essential for separating the ground state (1S) of Υ from its excited states (2S+3S). They are predicted to melt at very different temperatures.

Conventional muon detectors rely heavily on tracking stations, while this new detector proposes to use $<$100 ps timing and $\sim$1 cm spatial resolution to identify muons with momentum of a few GeV/c [4]. Multi-gap resistive plate chamber technology with large modules, long strips and double-ended readout (long-MRPC) was used for MTD prototype detectors. Similar technology but with small pads has been constructed and installed at STAR as a time-of-flight detector (TOF) [5]. In this paper, we present the conceptual design for the STAR MTD, the R& D results including the intrinsic timing and spatial resolution of long-MRPC and the MTD prototype performance at STAR. The muon identification capability and hadron background rejection are reported. Future perspectives for physics programs utilizing such detectors are discussed.

2. Simulation

The STAR detector was used for these studies [6]. The detector layout is shown in figure 1. The main tracking device is the time projection chamber (TPC) [7], whose inner and outer field cages are located at radial distances of 50 and 200 cm respectively from the beam axis. The TPC is 4 m long and it covers a pseudorapidity range $|\eta| < 1.8$ and 2π in azimuth. The ionization energy loss ($\mathrm{d}E/\mathrm{d}x$) is used for particle identification [8–10]. A TOF detector

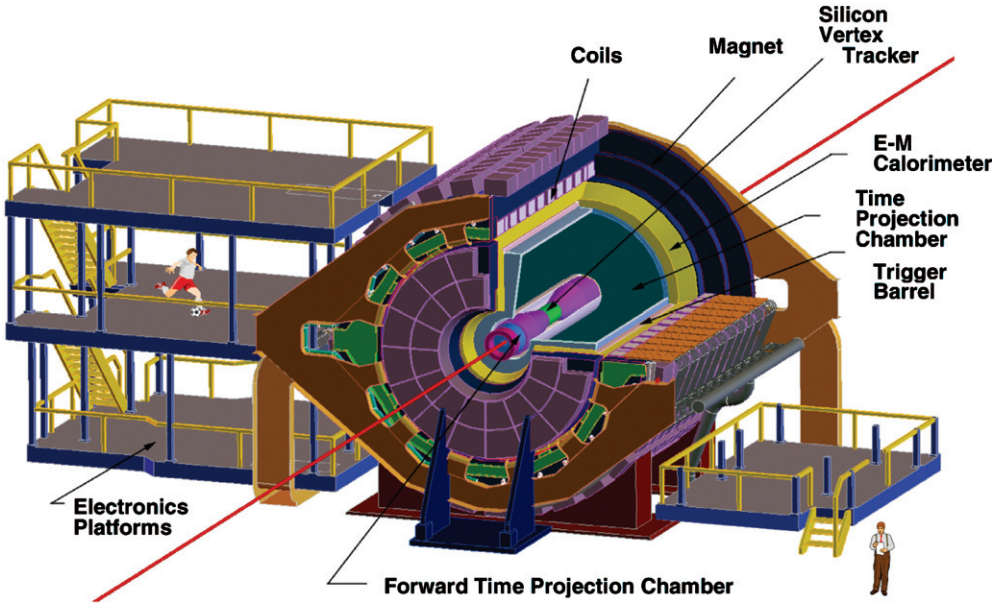

Figure 1. Perspective view of the STAR detector, with a cutaway for viewing inner detector systems. The trigger barrel, shown in this figure, will be fully replaced by the TOF detector in 2009. Figure is taken from [6].

based on multi-gap resistive plate chambers (MRPC) [11] will be fully installed in STAR in 2009, covering 2π in azimuth and $-1 < \eta < 1$ in pseudorapidity at a radius of ∼220 cm. It will extend particle identification up to $p_T \sim 3$ GeV/c for p and $\bar{p}$ [12]. The full barrel electromagnetic calorimeter (BEMC) is installed outside the TOF radius and uniformly covers $-1 < \eta < 1$ in pseudorapidity and 2π in azimuth [13]. The TPC is centered in a solenoidal magnetic field provided by the surrounding magnetic coils. The return flux path for the field is provided by the magnet steel [14], which is roughly cylindrical in geometry and consists of 30 flux return bars, four end rings and two poletips. The 6.85 m long flux return bars are trapezoidal in cross-section and 60 cm thick with a 363 cm outer radius. The width at the outer radius of the return bar is 57 cm.

The simulation of a full HIJING central Au+Au collision is shown in figure 2, using STAR geometry with a configuration of all the detectors and a complete material budget. We simulated a muon detector (in blue) covering the full return bars (in green) within $|\eta| < 0.8$ and left the gaps in-between return bars uncovered. This detector acceptance corresponds to 56% of 2π in azimuth. In figure 2, it can be seen that most of the particles are stopped before the BEMC and the few escaping particles (primary or secondary) mainly come through the gaps between the return bars.

Further simulation [15] with STAR geometry indicates that for a muon with $p_T > 2$ GeV/c generated in the center of the TPC, the detection efficiency of the MTD, including acceptance effects, is about 40–50%, while for a pion track, the efficiency is 0.5–1%. In this simulation, the charged tracks reconstructed in the TPC are extrapolated to the MTD and required to match the hit position as well as the time-of-flight from MTD measurements. We require the distance between the MTD hit and the projected point from the track to be within 4 cm and the timing difference to be less than 400 ps. It should be noted that in this study, a simple helix extrapolation of the track to the MTD was employed while in reality, the magnetic flux

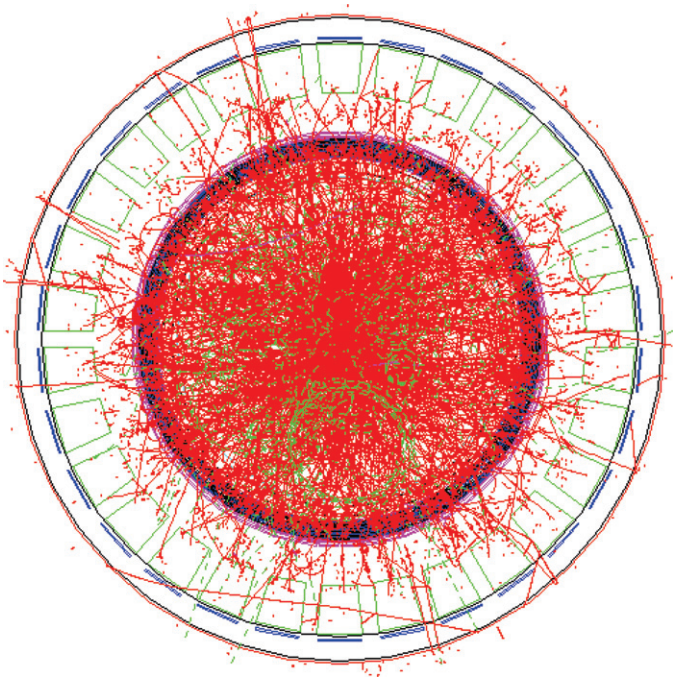

Figure 2. A full HIJING central Au+Au collisions simulated in STAR. The tracks in the TPC are projected in the plane transverse to the beam line.

return bar has a magnetic field of 1.2 tesla while the TPC has a 0.5 tesla field. Pion and kaon misidentifications come mainly from their decay into muons before the absorption by the return bar. These daughter muons then penetrate the return bars to reach the MTD. It is also evident from the simulations that protons are reduced by a much larger factor than pions and kaons. Shown in figure 3 is the combined acceptance and efficiency for primary muons, pions, kaons and protons. It indicates that the MTD can detect muons of $p_T \gtrsim 2$ GeV/c at a level of 45% while less than 1% of overall hadrons are accepted taking into account the relative yields of pions, kaons and protons. This illustrates that the MTD detector can reject hadrons effectively. A rejection factor of 50–100 can be obtained based on the simulations shown in figure 3 while maintaining an efficient trigger (>80%) for prompt muons. Further hadron rejection can be achieved with tracking in the TPC, $\mathrm{d}E/\mathrm{d}x$ in the TPC and hit matching in the TOF. These have been studied in detail with a prototype MTD tray in STAR. The results will be discussed in the next few sections. With the muon efficiency shown above and the measured $J/\psi p_T$ distributions [16], we obtained J/ψ efficiency versus p_T, as shown in figure 9.

3. The R&D results for the MTD

We utilize long-MRPCs for the detector design. Each long-MRPC module consists of two stacks of resistive glass plates resulting in a combined total of ten uniform gas gaps with gap widths of 250 μm. High voltage is applied to electrodes on the outer surfaces of the outer plates of each stack. A charged particle traversing a module generates avalanches in the gas gaps which are read out by six copper pickup strips with strip dimensions of 870 × 25 mm^2.

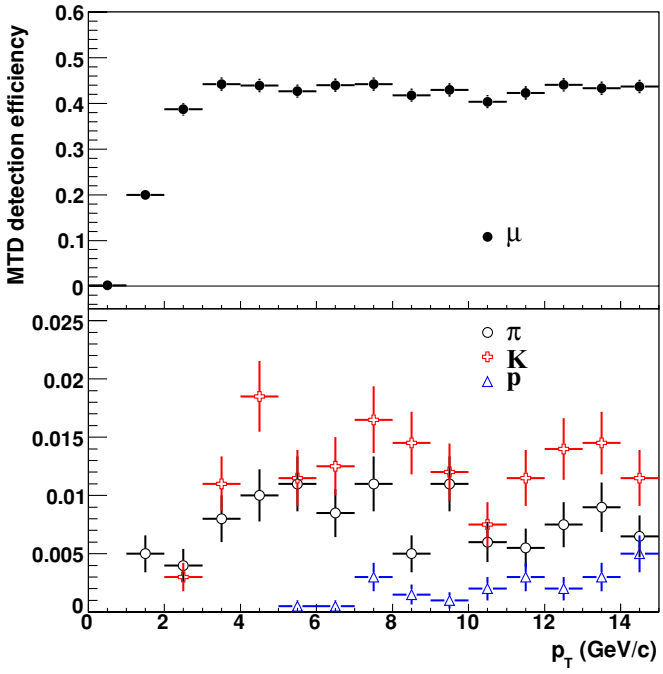

Figure 3. Efficiency for muons (top panel) and misidentification probabilities of pions, kaons and protons (bottom panel). The inefficiency for the muon is mainly due to the acceptance of the MTD (56).

The MRPC modules were operated at 12.6 kV with a mixture of 95% $C_2H_2F_4$ and 5% iso-butane at 1 atm. In the high-voltage range $12.5 < \mathrm{HV} < 13.0$ kV, the efficiency is above 95% and timing resolution is about 60–70 ps in the cosmic ray and beam tests. The spatial resolution of the long-MRPC along the long strip is about 0.6–1 cm in the same tests. This satisfies the needs for a large-area muon detector. The details of the long-MRPC construction and its performance in the cosmic ray and beam tests can be found in this paper [17].

4. Performances of a prototype MTD

A prototype of the MTD was installed and covered $\pi/60$ in azimuth and $-0.25 < \eta < 0.25$ in pseudorapidity at a radius of ∼400 cm during the 2007 run in 200 GeV Au+Au collisions. During the 2008 run in 200 GeV d+Au and p+p collisions, the prototype was re-located and covered $-0.5 < \eta < 0$ in pseudorapidity at the same radius. It contained two long-MRPC modules. The prototype was placed outside of the return bars which serve as a hadron absorber, each of which amounts to five interaction lengths. A mechanical drawing of the location and geometry of the MTD in STAR is shown in figure 4. The analog signals [18] were sent to trigger digitizer boards specially developed for use in the STAR trigger system [19] for signal amplitude and timing information read-out. Each digitizer board consists of an 8 bit analog-to-digital convertor (ADC). In addition, discriminator outputs from the digitizer boards with thresholds set to 30 mV were routed to a time-to-analog convertor (TAC), which was gated by the RHIC accelerator clock. The TAC signals were sent to a different channel of the digitizer board. Both ADC and TAC values were routed through the trigger distribution

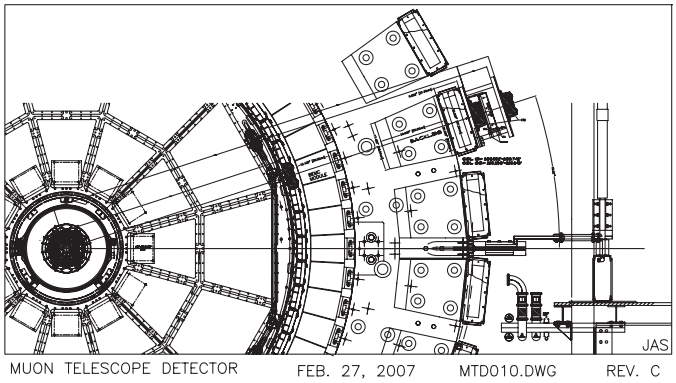

Figure 4. Position of the MTD prototype at STAR. The MTD was installed at 400 cm radially from interaction point in 2006–2008.

Table 1. Trigger rates, sampled luminosities, recorded events and matched hits with TPC tracks at $p_T > 1.5$ GeV/c in Au+Au, d+Au and p+p collisions in 2007 and 2008 with the prototype MTD.

Beam species	Interaction rate (Hz)	Trigger rate (Hz)	Sampled luminosity	Recorded events (M)	Matched hits
Au+Au	20 k	0.5–2	270 μb^{-1}	0.31	7 k
d+Au	100 k	0.5–2	29 nb^{-1}	1.6	78 k
p+p	300 k	0.5–2	404 nb^{-1}	0.56	8 k

and processing system for an initial (level 0) trigger decision [19]. The level 0 (L0) trigger is generated in less than 1.5 us from all the fast detector information available to trigger and is used to start the digitization process on slower detector systems (e.g. TPC). We have not required time difference or any other matching algorithms for a trigger decision as discussed in the simulation. A valid hit was required to have a non-zero and non-overflow ADC and TAC values within the 8-bit digitizer board range. The prototype successfully triggered the data acquisition system by requiring a valid hit in at least one strip of the long-MRPCs. Table 1 lists trigger rates, sampled luminosities and recorded events in Au+Au, d+Au and p+p collisions in 2007 and 2008 with the prototype MTD. For the 2009 run, we have installed another prototype tray, which is equipped with the same electronics as is used in the TOF system at STAR [5] to further improve the timing resolution of the MTD at STAR. The TOF electronics has a time bin width (25 ps) that is small compared to the detector resolution, and the degrading effects of the long cables are removed as the digitization will be done on-board the detector. The addition of the TOF-based electronics is expected to allow a significant improvement to the MTDs timing measurement in the off-line analysis.

Shown in figure 5 is the azimuthal angle distribution of particles from the TPC extrapolated to a radius of 400 cm in triggered d+Au collisions as a function of the transverse momentum p_T. The peak shows an enhancement of particle yield at the angle where the MTD is positioned. This shows that offline tracking of particles from the TPC was able to match hits from the long-MRPC. The tracks of the TPC were extrapolated to the MTD location, resulting in position information from tracking. The time difference from two-end readout of the hit strip provides a position measurement along the long strip of the long-MRPC. The MTD is placed behind the backleg steel of the magnet thus multiple hits are not an issue. The difference of these two

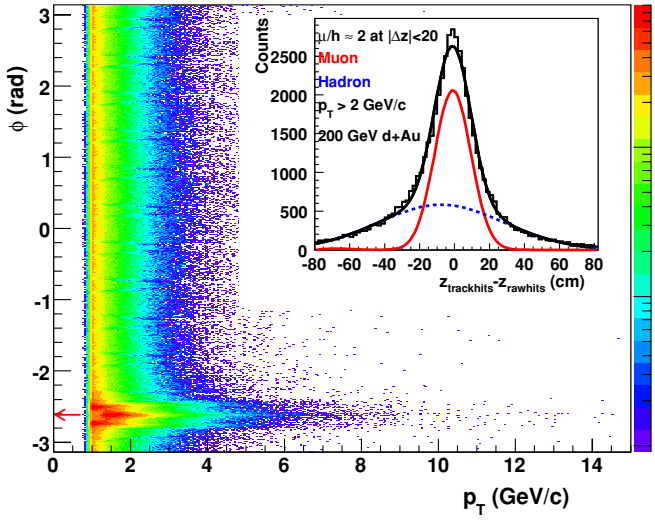

Figure 5. Azimuthal angle distribution of particles versus p_T in d+Au collisions, extrapolated from the TPC to a radius of 400 cm. The arrow denotes the azimuthal location of the prototype MTD tray. The inset shows Δz distribution. $z_{\text{trackhits}}$ is derived from extrapolation of the tracks of the TPC to the MTD location. z_{rawhits} is measured by the time difference from two-end readout of the hit strip along the long strip of the long-MRPC.

position values in the z-direction (Δz) is shown in the inset of figure 5, where the z-direction is the beam direction. A double Gaussian function was used to fit the distribution. σ of the narrow Gaussian was found to be ∼10 cm by selecting tracks of $p_T > 2\,\text{GeV}/c$ while the other Gaussian is significantly broader. The ratio of the particle yields in the narrow Gaussian to those in the broad Gaussian, within our match window at $|\Delta z| < 20$ cm (the narrow-to-broad ratio) is ∼2. Table 1 lists the total matched hits within the match window $|\Delta z| < 20$ cm at $p_T > 1.5\,\text{GeV}/c$ in Au+Au, d+Au and p+p collisions with the prototype MTD. From GEANT simulation, muons of $p_T \sim 2.5\,\text{GeV}/c$ generated at the center of the TPC result in a Gaussian distribution with a sigma of 9 cm in the z-direction in the MTD barrel, after traversing the detector materials from the TPC center to the MTD. The simulation also indicates that pions will result in a much broader distribution due to the strong interaction.

5. Muon identification capability and hadron rejection

At $p_T > 2\,\text{GeV}/c$, the $\text{d}E/\text{d}x$ of a muon track is ∼3–4% higher than that of a pion track [20]. The resolution of $\text{d}E/\text{d}x$ in the TPC is ∼8% [7], therefore, a half sigma difference in $\text{d}E/\text{d}x$ is expected between a muon and a pion track. About a two-sigma difference is expected between a muon and a kaon track. The energy loss due to multiple scattering in the return bar will cause an energy loss of ∼1.2 GeV for muons at $2 < p_T < 10\,\text{GeV}/c$ while the velocity change is negligible. For hadrons, the strong interaction will lead to a hadronic shower. This results in a significant energy loss and a change of velocity, and therefore a later arrival at the MTD. By selecting high velocity and large $\text{d}E/\text{d}x$ particles, the hadron background was observed to be significantly reduced and the narrow-to-broad ratio was found significantly enhanced. This is consistent with the expectation that the narrow Gaussian is dominated by muons and the broad Gaussian is dominated by hadrons. Within the match window $|\Delta z| < 20$ cm, muon purity can

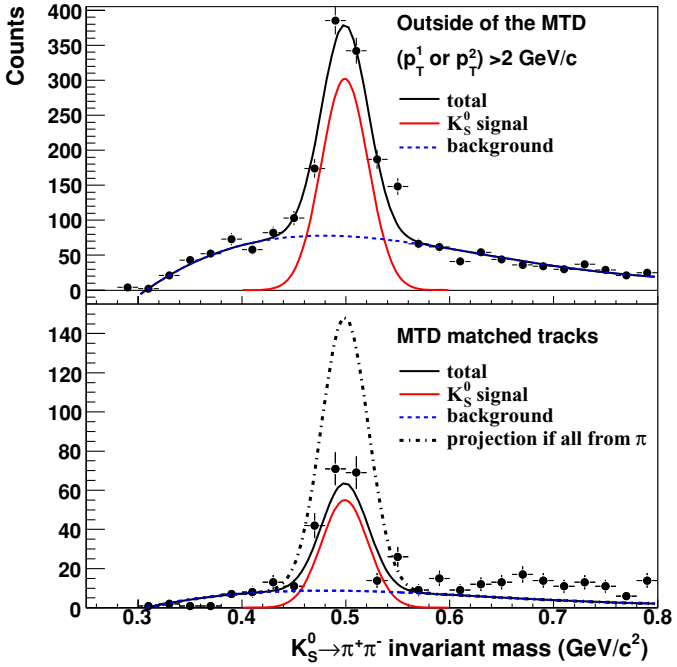

Figure 6. Reconstructed K^0_S which are not associated with MTD triggered particles (top panel); reconstructed K^0_S with at least one of the daughter pions associated with the MTD triggered particle. The dot-dashed line depicts the K^0_S yields from a projection assuming that the particles associated with MTD hits are all from pion decays (bottom panel).

be achieved to greater than 80% through the combined information of track matching, $\mathrm{d}E/\mathrm{d}x$, and velocity.

The average long-MRPC timing resolution for the two modules used in this analysis was measured to be ∼300 ps in Au+Au collisions. The 'start' time was provided by two identical vertex position detectors (VPDs), each 5.4 m away from the nominal collision point along the beamline [21]. After subtracting the start timing resolution (∼160 ps) and detector material effect contribution (∼100 ps at $p_T = 2.5$ GeV/c), the timing resolution (200–300 ps) from the MTD was found to be worse than those from cosmic and beam tests. This is understood by the fact that the trigger read-out electronics was not designed for precise time measurement. With the proposed full-scale detector, we will use TOF electronics. TOF electronics has a timing resolution of 25 ps. It has proved to be a low-cost, reliable system for recording timing information, reading it out and sending it to STAR DAQ. The electronics boards used for TOF can be used for the MTD efficiently, without any changes in design.

To further assess the pion contamination, we identify the pion tracks which come from the K^0_S weak decay through the hadronic decay channel $K^0_S \to \pi^+\pi^-$ to measure the fraction of muon candidates from pion decays. $K^0_S \to \pi^+\pi^-$ was reconstructed through decay V0 topology. Shown in figure 6 (top panel) is the raw K^0_S from pion pairs reconstructed in other azimuthal angles away from the MTD, while in the bottom panel is the raw K^0_S yield with at least one of the daughter pions associated with a MTD hit. The dot-dashed line depicts the K^0_S yields from a projection assuming that the particles associated with MTD hits are all from pion decays. We found the secondary muons from pion decay contributed 30–40% to the total muon candidates. The remaining background contaminating the prompt muon candidates was

Table 2. The fraction of TPC tracks which match with a non-zero EMC energy (> MIP) from non-MTD sectors (A), and the fraction of TPC tracks which match with a non-zero EMC tower energy (> MIP) and a MTD hit (B). A non-zero EMC energy is defined to be > 0.75 GeV above pedestal.

p_T (GeV/c)	EMC & non-MTD (A)	EMC & MTD (B)
1.5–2	$(2.21 \pm 0.03)\%$	$(0.18 \pm 0.02)\%$
2–3	$(3.67 \pm 0.07)\%$	$(0.30 \pm 0.04)\%$
3–4	$(5.89 \pm 0.22)\%$	$(0.34 \pm 0.10)\%$
4–6	$(7.92 \pm 0.50)\%$	$(0.65 \pm 0.24)\%$

secondary muons from kaon decay. This can be investigated using the difference of TPC track $\mathrm{d}E/\mathrm{d}x$ for kaons and muons. By cutting on a high $\mathrm{d}E/\mathrm{d}x$ value of $n\sigma_\pi > 0$, where $n\sigma_\pi$ is the measured $\mathrm{d}E/\mathrm{d}x$ normalized by the value of expected pion $\mathrm{d}E/\mathrm{d}x$ [8], we reject part of the kaon secondary decay products. Furthermore, from p+p MTD triggered events taken in 2008, we found that the inclusive muon yields can be decreased by a factor of 2 by requiring a coincidence with a valid hit in the TOF system in the same TPC sector.

We not only use several detectors (TPC, TOF and MTD) to improve the muon identification, but also use additional detectors to check the performance of hadron rejection. One of the methods is to use hadronic showers in the BEMC to study the fraction of inclusive muon candidates from hadron showers starting at the EMC and penetrating the absorbers. Only a few percent of hadrons produce showers and deposit energy above the minimum ionization energy (MIP) in the BEMC. Table 2 shows the fraction of hadrons with energy deposited in the BEMC greater than 0.75 GeV with and without any MTD hit associated. There is a factor of $\geqslant$10 reduction of hadronic shower in the BEMC when we require muon candidacy in the MTD. Since the electron yield is about 0.1% of the inclusive hadron yield in 2008 in 200 GeV p+p collisions at STAR [24], it is reasonable to assume that all the BEMC showers with a TPC track are hadrons when a MTD hit is not associated. This means that the contribution from hadrons was reduced from $\simeq$100% to $\leqslant$10% while that from muons (both prompt and from hadron decays) increased to $\geqslant$90% of the remaining sample. By comparing the difference between the BEMC showers with and without the MTD hit requirement, we conclude that particles which arrive at the BEMC when there is a valid MTD hit in coincidence are indeed mostly dominated by muons. However, the muons are primarily from pion and kaon decays in the first 2 m of the STAR detector.

Since the prompt muons are predominantly from charm semi-leptonic decay, we compare our muon yields to non-photonic electron yields in the same p_T bin to assess the muon contamination from pion and kaon decays. The raw yields of muons were obtained from Gaussian fits to the distributions of Δz. The narrow component is attributed to the muon. The systematic uncertainty on the muon raw yields from different fit ranges and parameter constraints is about 20%. The acceptance and efficiency were studied in simulations and corrected for the yields. The ratio of the raw yields $\mathrm{d}^2N/(2\pi p_T dp_T dy)$ of inclusive muons $((\mu^+ + \mu^-)/2)$ to the non-photonic electron yields in 200 GeV d+Au collisions at mid-rapidity is shown in figure 7 for different muon selection criteria. Also shown in figure 7 is the pion related contribution to the inclusive muon yield as a function of p_T, evaluated by reconstructing K^0_S with at least one of the daughters associated with the MTD hit, as described above in detail. The non-photonic electron invariant yields are from STAR publications [22]. Compared to the non-photonic electron yields, the primary muons contributed 6–10% to the inclusive muons if only MTD hit association was applied. Table 3 lists the primary muon selection efficiency

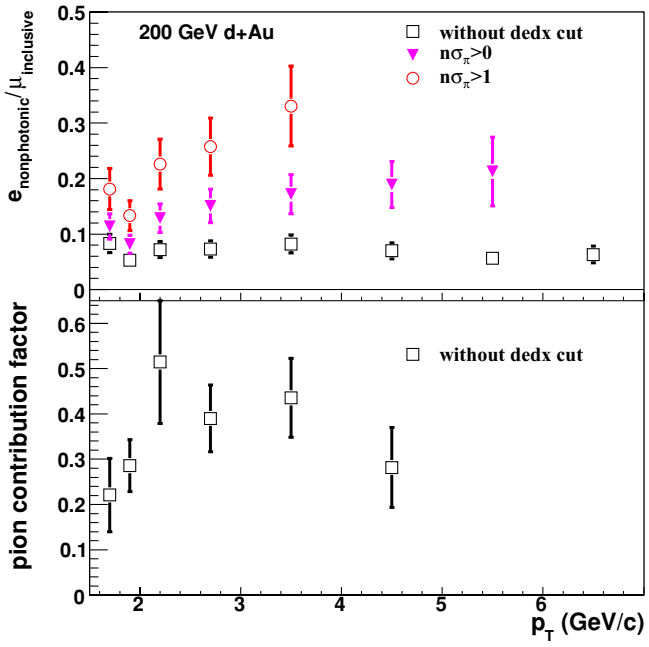

Figure 7. Estimation as a function of p_T of the fraction of detected muons which are prompt by comparison of the total inclusive muon yield to the measured yield of non-photonic electrons (electrons not resulting from photon conversion, hadron decays or Dalitz decays). The estimate is made with and without cuts on the ionization energy loss (relative to that expected for a pion) in the TPC for the track projected to the position of the MTD. Since $\mathrm{d}E/\mathrm{d}x$ for a muon in the relevant momentum range is higher than that for a pion, increasing the cut on $n\sigma_\pi$ results in a higher fraction of prompt muons (top panel); the contribution from pion decays to the measured inclusive muon signal as a function of p_T, determined by measuring the MTD response when a pion from a K^0_S decay enters its acceptance (bottom panel).

Table 3. The signal-to-background ratio and primary muon selection efficiency under different conditions in 200 GeV d+Au collisions. The S/B ratio is p_T dependent.

Selection criterion	Primary muon efficiency (%)	S/B ratio
Without cut	100	1/15–1/9
$n\sigma_\pi > 0$	61	1/10–1/6
$n\sigma_\pi > 1$	26	1/6–1/3

and the ratio of primary muon over secondary muon from pion and kaon decays (S/B) under different selection criteria on $\mathrm{d}E/\mathrm{d}x$. By selecting on a high $\mathrm{d}E/\mathrm{d}x$ value of $n\sigma_\pi > 1$, the S/B ratio increased by a factor of 3, as shown in table 3.

6. Trigger capability

The full muon telescope detector will cover 56% of the TPC acceptance at $|\eta| < 0.8$. If the similar design as for the prototype tray is used, there will be 540 long-MRPC modules, 2160 read-out strips and 4320 read-out channels, which is a factor of 5–6 less than what have been used for the TOF at STAR. By using the same electronics design, the expense for the full

Table 4. The trigger rate reduction by requiring a single hit or double hits in the MTD for different collision systems at 200 GeV with full MTD coverage. L0: single-hit L0 rate output from MTD for a given collision event; L2 with TOF: single-hit rate reduction at L2 trigger with requirement of a TOF hit at the vicinity of the path of a muon candidate (the rate in p+p collisions is measured; the rate in central Au+Au collisions is estimated only); RHIC II Lumi: RHIC II luminosity in terms of collision rate; dimuon L2 rate: dimuon trigger rate at L2 in hertz at the RHIC II. The numbers in the parentheses are from simulations with a tighter timing cut assuming the electronics can provide ∼100 ps resolution.

Collision system	L0	L2 with TOF	RHIC II Lumi (Hz)	Dimuon L2 rate (Hz)
Minbias Au+Au	0.2	–		
0–5% Au+Au	0.5 (0.2)	∼0.3	100 k	∼500 (100)
60–80% Au+Au	0.03	–		
d+Au	0.02	–		
p+p	0.01	0.003	2 M	$\leqslant$10

coverage of MTD system will be very cost effective and will likely be similar in scope to the smaller RHIC II upgrades.

Based on the MTD trigger rate from the prototype tray in Au+Au collisions in 2007, we estimate for the full coverage the L0 trigger rate reduction for a single MTD hit will be 0.19 in minimum-bias Au+Au collisions. Therefore, online trigger enhancement for di-muon trigger will reach 28. From 1 billion minimum-bias Au+Au events, corresponding to 36 million di-muon triggered events, we expect to get 5600 J/ψ and 85 Υ through di-muon decays. Table 4 lists the L0 trigger rate reduction for a single MTD hit with full MTD coverage in different collision systems, which were estimated from the trigger rates and enhancement factors for the prototype MTD tray in 200 GeV Au+Au collisions in 2007 and d+Au and p+p collisions in 2008. Table 4 also indicates the trigger capability in central Au+Au collisions for the di-muon program. In p+p collisions it was found that when there was a coincidence with the hit in the TOF detector in the same TPC sector, the trigger rate was reduced by a factor of 3. From the extrapolation of a valid MTD hit and the time difference measured between the VPDs on the east and west sides of the interaction point, the expected hit position in the TOF system was obtained. From the TOF system, the module ID with a valid hit leads to another position measurement since the modules in the TOF system are sequentially positioned along the z-direction. Shown in figure 8 (left panel) is the extrapolated z position versus measured module ID with a valid hit in the TOF system in 200 GeV p+p collisions. Strong correlations were observed. The difference of these two z values is shown in the right panel of figure 8. A single Gaussian was used to fit the distribution and the sigma was found to be ∼6 cm. Combining the information in the MTD and TOF systems, we can obtain an order of magnitude rejection dramatically increasing the efficiency for dimuon triggers in central Au+Au collisions at 200 GeV.

7. Physics perspectives with full coverage

In this section, we explore the physics potential of a full coverage MTD for STAR at mid-rapidity. Two physics cases are selected to illustrate the MTD capability for online triggering and improvement of momentum resolution to achieve physics goals of measuring J/ψ elliptic flow and R_{AA} at high-p_T and resolving ground state of Υ from its excited states. In addition,

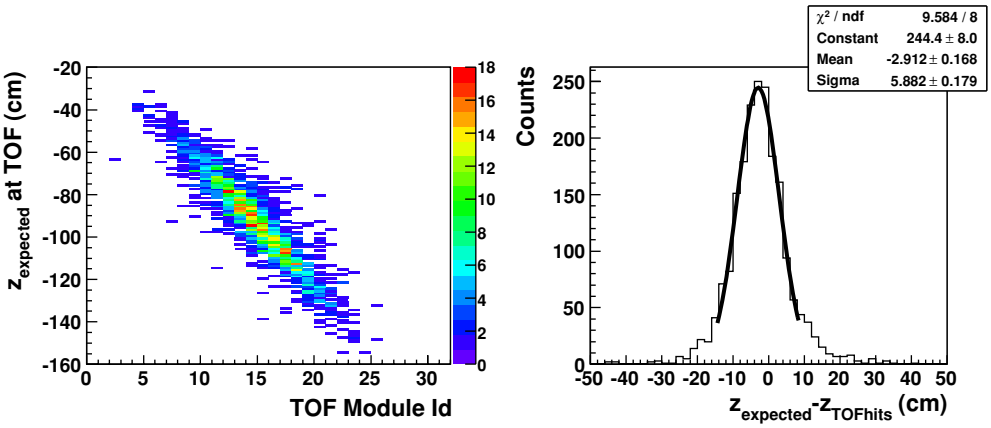

Figure 8. The expected z position at the TOF system versus the module ID with a valid hit in 200 GeV p+p collisions in 2008. The modules in the TOF system are sequentially positioned along the z-direction (left panel); the distributions of the difference between the expected position and the measured position along the z-direction from the TOF system (right panel). The expected position (z_{expected}) is obtained from the extrapolation of a valid MTD hit and the time difference measured between the VPDs on the east and west sides of the interaction point.

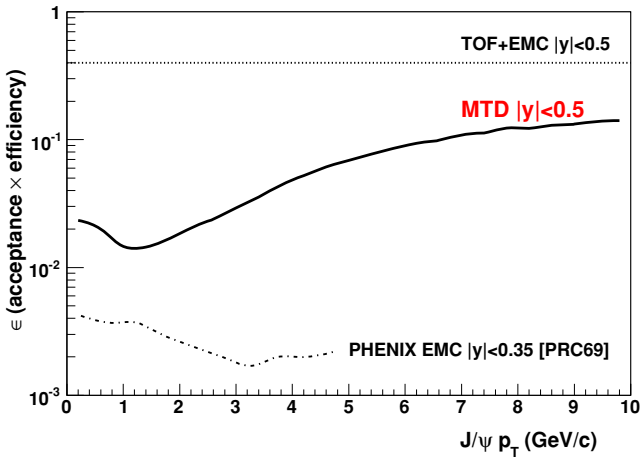

Figure 9. Efficiency for J/ψ as a function of p_T. PHENIX [23] and STAR detect $J/\psi \to e^+e^-$ at mid-rapidity using a combination of several detectors together with electromagnetic calorimeters.

electron–muon correlation can be used to distinguish lepton pair production from heavy quark decays ($c + \bar{c} \to e + \mu(e)$, $B \to e(\mu) + c \to e + \mu(e)$).

Shown in figure 9 are the efficiencies for J/ψ at mid-rapidity at the RHIC. Both PHENIX and STAR are able to detect J/ψ at mid-rapidity through $J/\psi \to e^+e^-$ with electromagnetic calorimeters as trigger device and electron identifier. However, this is limited by the capability to trigger on electrons at low momentum in STAR and relatively lower efficiency times acceptance (ϵ) in PHENIX [23]. The proposed MTD detecting $J/\psi \to \mu^+\mu^-$ will have much higher trigger rejection power over the STAR EMC and TOF combination and have larger acceptance over PHENIX configuration. This results in much larger J/ψ sample than the currently available RHIC experimental setups.

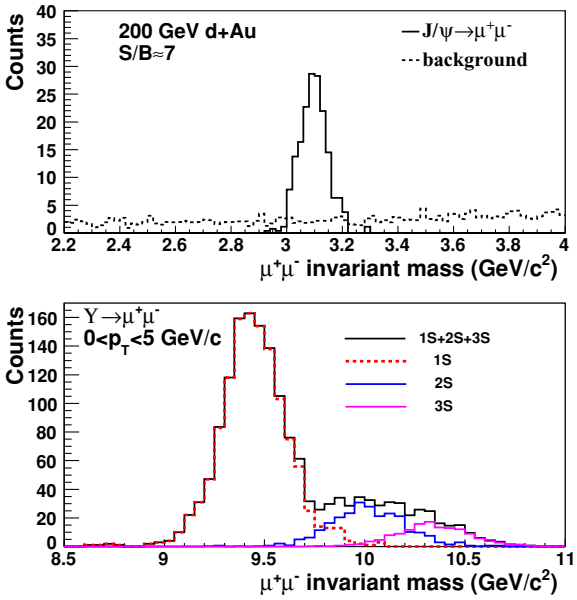

Figure 10. The expected di-muon invariant mass distribution from J/ψ and background in d+Au collisions (top panel); the invariant mass distribution of di-muon decayed from Υ at $0 < p_T < 5$ GeV$/c$ (bottom panel). The different Υ states can be separated. The background at Υ mass range is not simulated since our small acceptance prototype has not provided high enough p_T reach.

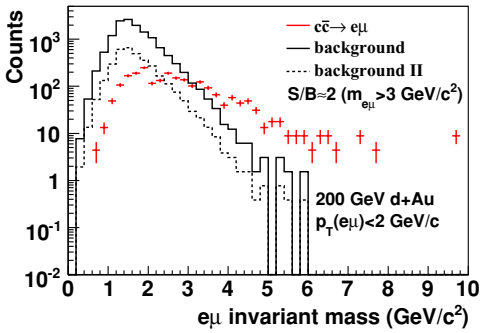

Figure 11. The expected electron–muon correlation from charm pair production and from random background in d+Au collisions. The statistics shown are equivalent to 2 billion minbias d+Au collisions.

Shown in figure 10 (top panel) is $J/\psi \rightarrow \mu^+\mu^-$ with a signal-to-background ratio of 7:1. The background di-muon pairs are simulated from the inclusive muon yields obtained from studies shown in previous sections. Shown in figure 10 (bottom panel) is the invariant mass distribution of di-muons decayed from Upsilon, simulated in the STAR geometry. Clearly, different Upsilon states ($\Upsilon(1S)$, $\Upsilon(2S)$ and $\Upsilon(3S)$) can be separated through the di-muon decay channel while bremsstrahlung energy losses of electrons present a challenge for the separation due to the detector materials with future inner tracker upgrades at STAR. Shown in figure 11 are the simulation results of the electron muon invariant mass distribution from charm pair production and from background. The cross symbols represent the signal. The solid

line represents the background, obtained using random combinations between the photonic electron yields measured in d+Au collisions [24] and inclusive muon yields shown in previous sections. The signal-to-background ratio for charm pair production is 2:1 if the invariant mass of the electron muon pair is larger than 3 GeV/c^2 and p_T is less than 2 GeV/c. The photonic electrons can be paired with other particles in the TPC, which will lead to a factor of 2 rejection. The inclusive muons can be associated with the TOF hits, resulting in at least another factor of 2 rejection. If we include these rejection factors, the background will be reduced by a factor of 4, as shown by the dashed line. The signal-to-background ratio for electron muon correlation is significantly enhanced.

In the RHIC II era, when 26 nb^{-1} and 300 pb^{-1} luminosity for Au+Au and p+p collisions are delivered, we expect to get 169 k J/ψ and 2500 Υ in p+p collisions, and 630 k J/ψ and 9300 Υ in Au+Au collisions [25]. These measurements are essential to advance our understanding of the QCD matter created at the RHIC.

8. Conclusions

In summary, we propose a large-area, cost-effective muon telescope detector for STAR and for the next generation of detectors at a possible electron-ion collider. Cosmic ray and beam tests show the intrinsic timing resolution of the long-MRPC is about 60–70 ps and spatial resolution is better than 1 cm. The prototype of the MTD tray triggered the data acquisition system at STAR successfully. The results showed that offline tracking of particles from the TPC was able to match hits from the long-MRPC. A muon purity of $> 80\%$ can be achieved. The ratio of primary muon over secondary muon was studied and found to be of high quality for the quarkonium program at the RHIC.

Acknowledgments

We thank the STAR Collaboration and the RCF at BNL for their support. This project is supported by the BNL Laboratory directed R& D fund 07-007. Long-MRPC R&D at USTC is supported by the National Natural Science Foundation of China (10775131). LR thanks the Battelle Memorial Institute and Stony Brook University for the support in the form of the Gertrude and Maurice Goldhaber Distinguished Fellowship. Z Xu is supported in part by the PECASE Award.

References

[1] Adams J *et al* 2005 *Nucl. Phys.* A **757** 102
[2] Arsene I *et al* 2005 *Nucl. Phys.* A **757** 1
Adcox K *et al* 2005 *Nucl. Phys.* A **757** 184
Back B B *et al* 2005 *Nucl. Phys.* A **757** 28
[3] Rapp R and Wambach J 2000 *Adv. Nucl. Phys.* **25** 1
Matsui T and Saltz H 1986 *Phys. Lett.* B **178** 416
Electromagnetic Probes at RHIC II (Working Group Report) David G, Rapp R and Z Xu 2008 *Phys. Rep.* **462** 176
[4] Z Xu *BNL LDRD project 07-007; Beam Test Experiment (T963) at FermiLab*
[5] STAR Time-of-Flight Proposal: http://www.star.bnl.gov/STAR/tof/publications/TOF_20040524.pdf
[6] Ackermann K H *et al* 2003 *Nucl. Instrum. Methods* A **499** 624
[7] Anderson M *et al* 2003 *Nucl. Instrum. Methods* A **499** 659
[8] Shao M *et al* 2006 *Nucl. Instrum. Methods* A **558** 419
[9] Bichsel H 2006 *Nucl. Instrum. Methods* A **562** 154
[10] Xu Y *et al* arXiv:0807.4303

[11] Bonner B *et al* 2003 *Nucl. Instrum. Methods* A **508** 181
Shao M *et al* 2002 *Nucl. Instrum. Methods* A **492** 344
J Wu *et al* 2005 *Nucl. Instrum. Methods* A **538** 243
[12] Adams J *et al* 2005 *Phys. Lett.* B **616** 8
[13] Beddo M *et al* 2003 *Nucl. Instrum. Methods* A **499** 725
[14] Bergsma F *et al* 2003 *Nucl. Instrum. Methods* A **499** 633
[15] Lin G (for the STAR Collaboration) 2006 *A New Large-area Muon Telescope Detector at Mid-rapidity at RHIC, talk presented at DNP 2006, Nashville, TN, 25–28 October*
[16] Tang Z (for the STAR Collaboration) 2008 QM2008 Proc. *J. Phys. G: Nucl. Part. Phys.* **35** 104135 (arXiv:0804.4846)
Abelev B I *et al* 2009 *Phys. Rev. Lett.* submitted (arXiv:0904.0439)
[17] Sun Y *et al* 2008 *Nucl. Instrum. Methods* A **593** 307
[18] Llope W J *et al* 2008 *Nucl. Instrum. Methods* A **596** 430
[19] Bieser F S *et al* 2003 *Nucl. Instrum. Methods* A **499** 766
[20] Eidelman S *et al* 2004 *Phys. Lett.* B **592** 1
[21] Llope W J *et al* 2004 *Nucl. Instrum. Methods* A **522** 252
[22] Adams J *et al* 2005 *Phys. Rev. Lett.* **94** 62301
Abelev B I *et al* 2007 *Phys. Rev. Lett.* **98** 192301
[23] Adler S S *et al* 2004 *Phys. Rev.* C **69** 014901
[24] Jin F (for the STAR Collaboration) SQM2008 Proc. arXiv:0901.0693
[25] Frawley A D, Ullrich T and Vogt R 2008 *Phys. Rep.* **462** 125